Convergence and robustness of the Hopf oscillator applied to an ABLE exoskeleton: reachability analysis and experimentation

Abdelwaheb Hafs[1,2], Dorian Verdel[1,2], Jawher Jerray[3], Olivier Bruneau[4], Nicolas Vignais[1,2], Bastien Berret[1,2,5] and Laurent Fribourg[6]

[1] CIAMS, Université Paris-Saclay, Bât. 335, Bures-sur-Yvette, 91405 Orsay cedex, France
{abdelwaheb.hafs, dorian.verdel, nicolas.vignais, bastien.berret}@universite-paris-saclay.fr
[2] CIAMS, Université d'Orléans, Orléans, France
[3] LTCI, Télécom Paris, Institut Polytechnique de Paris, Sophia-Antipolis, France
jawher.jerray@telecom-paris.fr
[4] LURPA, ENS Paris-Saclay, 4 Av. des Sciences, Gif-sur-Yvette, 91190, France
olivier.bruneau@ens-paris-saclay.fr
[5] Institut Universitaire de France, Paris, France
[6] University Paris-Saclay, CNRS, ENS Paris-Saclay, LMF, F-91190 Gif-Sur-Yvette, France
fribourg@lsv.fr

Abstract

In this paper, we consider an industrial exoskeleton called ABLE, which we controlled using an adaptive oscillator. In the context of periodic human movements around the elbow axis we show that the exoskeleton anticipates smoothly the human movement, converges towards a limit cycle, and is "robust" against non-deterministic bounded perturbations. In particular, the properties of stability and robustness are formally proven, at the model level, using a recent development of the method of "reachability analysis". These properties are then confronted to preliminary experimental data.

1 Introduction

Active exoskeletons are wearable robotic devices, developed to assist human movement [1, 13]. Their versatility makes it possible to consider numerous applications, in particular to improve rehabilitation protocols [9, 10, 19, 21, 23] and to prevent musculoskeletal disorders in workers [5, 6, 22, 29]. The implementation of exoskeletons for these different applications is nevertheless constrained by the impossibility of completely predicting human movement intention [1, 14]. Several approaches have been proposed in the literature to solve this problem. The first approach relies on controllers based on bioelectric signals such as electromyography [30, 31] or electroencephalography [7]. Other biological signals such as gaze were also included in the control strategies to detect human intention [20]. All these strategies rely on the appearance of the signals considered before the appearance of the movement kinematics, which is called electromechanical delay in the case of myoelectrical signals. Another proposed approach was to learn the human movement [14], which led to a significant reduction of unwanted interaction efforts in reaching movements. In the case of periodical movements, approaches based on adaptive oscillators have been proposed and successfully experimented [24–27]. At the theoretical level, the authors of [25] proved the stability of the model of one of these oscillators: the Hopf oscillator. The proof uses the classical "perturbation method" that consists in introducing an infinitesimal perturbation ε in the model, expressing the solution as a power series in ε, and showing the positiveness of the radius of convergence of the series. The Hopf oscillator is also considered here, but the stability is proven by introducing a *bounded perturbation w* (instead of an infinitesimal perturbation ε) taking its values

non-deterministically in a given set $\mathscr{W}$ of the form $[-c;c]$ with $c>0$. In order to show the stability of the system in presence of such perturbations, we make use of a recent development of the method of "reachability analysis" (see [2] for a survey). Given an initial set of states S_0, this method constructs iteratively by "set-based integration" the set S_1 of the states reached at the end of one time step, then S_2 at the end of a new time step, etc. These sets $S_1;S_2;...$ are over-approximations of the exact sets of solutions of the system, for any initial state in S_0 and for any admissible perturbation taking its values in $\mathscr{W}$. When one succeeds in generating a finite representation of the set $\mathscr{I} := \cup_{i=0}^{\infty} S_i$, one obtains a description of a superset of all the states that can be reached from S_0. The set $\mathscr{I}$ is an invariant set of the system: the trajectory from any point of $\mathscr{I}$ remains in $\mathscr{I}$ indefinitely (see [4]). We explain here how to successfully generate such a set $\mathscr{I}$ for the Hopf oscillator. In the present paper, this previously defined oscillator [27] is applied to an upper-limb exoskeleton to design a transparent control. Transparency is defined as the interaction between the human and the exoskeleton with minimum efforts. Our primary contributions lie in formally proving the convergence and stability of the oscillator and validating this proof through experimental results. The theoretical development allows a priori evaluation of whether the system converges to a limit cycle and is robust to non-deterministic bounded amplitude disturbances. In particular, the experiments have confirmed the invariance property of the set $\mathscr{I}$: once a first experimental datum relative to the arm position lies in $\mathscr{I}$, all the subsequent data also lie in $\mathscr{I}$. In the present study, the transparent control mode is chosen to experimentally evaluate the stability of the oscillator, independently from model errors that can appear when using assistance control modes and that can lead to instability [27]. In this control mode, the human movement should be impacted as little as possible by the exoskeleton [1, 3, 14, 32]. The experiments are conducted on elbow flexion/extension with an upper-limb exoskeleton called ABLE [11, 29] (see Section 2.2 for details).

2 Material and methods

2.1 Adaptive oscillators

As mentioned in the introduction, human intention prediction may be achieved by adaptive oscillators for periodic movements. These oscillators allow to estimate the fundamental parameters (amplitude and frequency) of arbitrary rhythmic signals in a supervised learning framework. Among different types of adaptive oscillators, we focus here on the Hopf oscillator, which is one of the most widely used types in the field of robotics and assistive technology [27] [25] [34] [37].

The Hopf oscillator is defined by a system of two differential equations (Eq. (1)).

$$\begin{cases} \dot{x}(t) = \gamma(\mu - r^2)x(t) - \omega(t)y(t) + \nu e(t) \\ \dot{y}(t) = \gamma(\mu - r^2)y(t) + \omega(t)x(t) \end{cases} \tag{1}$$

With $r = \sqrt{x^2+y^2}$, where $x(t)$ and $y(t)$ are the orthogonal coordinates of the oscillator, e is the oscillator's external force, ν the *coupling gain*, μ and γ are the amplitude and attractiveness of the oscillator respectively [26]. For this study $\gamma = 1$ (as in [25–27]), and $\mu = 1$ (so that the intrinsic amplitude of the oscillator is equal to 1).

The input of the oscillator is the real position θ. In this case the external force of the oscillator e represents the difference between the real position θ of the human elbow and the estimated position $\hat{\theta}$.

Righetti and Ijspeert [24] augmented this oscillator to learn the frequency ω, amplitude α_1 and offset

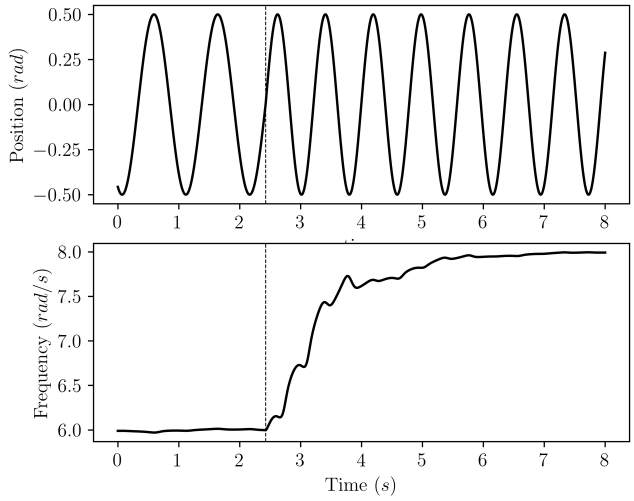

Figure 1: Example of oscillator's adaptation. Top panel: the oscillator's input. Bottom panel: evolution of the learned frequency

α_0 of the input using integrators. The complete estimation algorithm is presented in Eq. (2)

$$\begin{cases} \dot{\omega}(t) = -\nu e(t)\sin(\phi(t)) \\ \dot{\phi}(t) = \omega(t) - \nu e \sin(\phi(t)) \\ \dot{\alpha}_1(t) = \eta cos(\phi(t))e(t) \\ \dot{\alpha}_0(t) = \eta e(t) \\ \hat{\theta}(t) = \alpha_0(t) + \alpha_1(t)\cos(\phi(t)) \end{cases} \tag{2}$$

Where η is the *integrator gain* and ϕ the output phase. Finally the estimated position $\hat{\theta}$ is used to compute the torque generated by the exoskeleton to assist the human movement (see Section 2.2 for details).

2.2 Exoskeleton modeling

ABLE is an upper limb exoskeleton. This exoskeleton is based on a screw and cable transmission allowing high levels of reversibility and transparency [11, 12]. It has four active degrees of freedom (see Fig. 2). The first three correspond to rotations of the human shoulder, the fourth correspond to rotation of the elbow (flexion/extension). The physical interfaces between the exoskeleton and the user include passive rotations and translation to minimize undesired efforts due to the connection hyperstatism [15, 28]. Additional settings are available to adapt the exoskeleton to the user. The robot is mounted on a fixed frame with a winch to adapt its height.

The proposed method consists of using the joint position and velocity estimated by the oscillator instead of the measured position and velocity. As we focus on the last axis (elbow), the inverse dynamic model of the robots elbow axis is computed upon the basis of classical robot dynamics [32, 33]. and represented in Eq. (3).

$$\begin{aligned} \hat{\tau}_m = &(g(-x_m\cos(\hat{\theta}) - y_m\sin(\hat{\theta})) \\ &+ \dot{\hat{\theta}}\mu_v + sign(\dot{\hat{\theta}})\mu_c)\frac{1}{r} \end{aligned} \tag{3}$$

Figure 2: Exoskeleton ABLE

Here $g = 9.81$ m/s^2 the gravity acceleration, (x_m, y_m) the exoskeleton's forearm centre of gravity coordinates, μ_v the friction coefficient, μ_c the Coulomb dry friction coefficient, $\hat{\tau}_m$ the estimated motor torque, and r the torque reduction ratio.

Finally Fig. 3 represents the exoskeleton control scheme. The position θ is measured by exoskeleton internal sensors. As shown, the oscillator's input depends on both the control law and the modulation performed by the human, where the human central pattern is represented by the transfer function on the feedback loop.

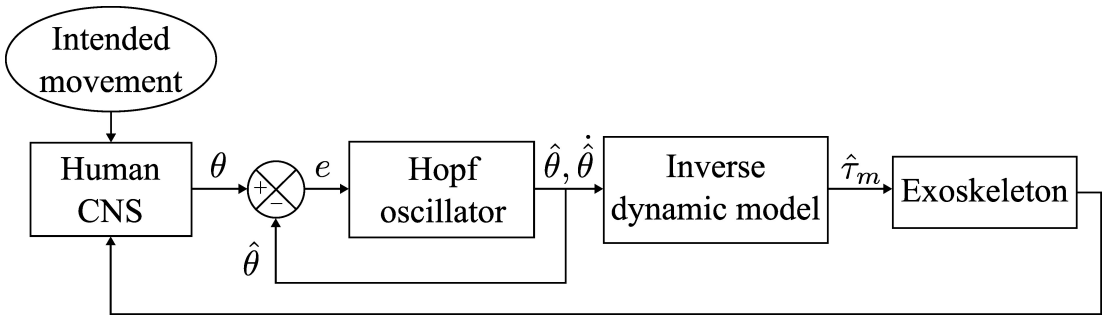

Figure 3: Exoskeleton Control scheme

3 Reachability Analysis

We focus here on *sinusoidal* inputs (corresponding to sinusoidal movements of the users) with bounded uncertainty.

The stability of the Hopf oscillator was proved in [25] using the "perturbation method". The perturbation method was developed in the 19th century by Laplace and others to show, for example, the orbital stability of the moon around the Earth despite the influence of the sun. Roughly speaking, the equation of the ideal motion (without perturbation) is modified by injecting an infinitesimal value ε, and the solution of the modified equation is expressed as a power series in ε. The stability is demonstrated by showing that the radius of convergence of the series is non-zero. We prove here the stability of the Hopf oscillator using the method of "reachability analysis". Reachability analysis has been developed since a couple of decades in the community of formal methods and model checking (see [2] for a recent review). In this method, one is given a set S_0 of initial points and a perturbation w, which is not infinitesimal as in the perturbation method, but of bounded amplitude (typically $w \in \mathscr{W} = [-c,c]$ with $c > 0$). Reachability analysis then constructs by "set-based integration" first the set S_1 of the states reached at the end of one time step, then S_2 at the end of a new time step, etc. These sets $S_1, S_2, \ldots$ are over-approximations of the exact sets of solutions of the system, for any initial state in S_0 and for any admissible perturbation taking its values non-deterministically in $\mathscr{W}$. The set $\bigcup_{k=0}^{K} S_k$ characterises a superset of all the states on the time interval $[0, Kh]$, where h is the time-step size. This set is often referred to as the "reachability tube".

In the case where we can detect that at a time $t = Lh$ for some $L \in \mathbb{N}$, the set of states S_L is contained in the tube currently generated ($S_L \subset \bigcup_{k=0}^{L-1} S_k$), we obtain a *finite* representation of a superset of all the states that can be reached from S_0. The set $\mathscr{I} = \bigcup_{k=0}^{L} S_k$ is an *invariant set* of the system: the trajectory from any point of $\mathscr{I}$ remains in $\mathscr{I}$ indefinitely (see [4]).

For an oscillatory system, this invariant set is shaped like a tube rounding on itself (a "doughnut" in 3D). In [8], we represented the set S_k as a ball $B(y_k, \delta(k))$ of centre y_k and radius $\delta(k)$. The centre y_k of the ball $B(y_k, \delta(k))$ is the value computed by Euler's explicit method at the k-th step. The radius $\delta(k)$ is determined by an analytical formula giving an upper bound on the error introduced by Euler's method (see [8]). The detection of the inclusion $S_L \subseteq \bigcup_{k=0}^{L-1} S_k$, is done by finding a value K such that

$$B(y_L, \delta(L)) \subseteq B(y_K, \delta(K))$$

with $L = K + \ell h$ for some integer ℓ. The value $T = \ell h$ is the estimated value of the system period (see [18] for details). The invariant set $\mathscr{I} = \bigcup_{k=0}^{L} S_k$ is here a looping tube, centred on a set of values $y_0, y_1, \ldots, y_L$ corresponding to the "limit cycle" $\mathscr{C}$ of the system.

The main advantage of the reachability analysis over the perturbation method is its ability to take into account perturbations of a given amplitude, and to construct an invariant set $\mathscr{I}$ in which the state of the system is guaranteed to be confined. This allows us to characterize the "robustness" of the system against bounded perturbations.

Our method of reachability analysis has been implemented in Python in a software called ORBITADOR. The method has been successfully applied to various systems, for example we have shown the stability of a parametric Van der Pol system in [17] and a biochemical process model in [18]. We also studied the stability of hybrid systems such as the passive biped model in [16]. Here ORBITADOR is applied to the system Eq. (2) for $\mathscr{W} = [\frac{-2\pi}{4000}, \frac{2\pi}{4000}]$(which corresponds to the true sensitivity of the optical sensors embedded in the exoskeleton), $h = 10^{-3}$ (which corresponds to the real time sampling frequency of exoskeleton control), $\delta_0 = 0.084$, and the initial condition $x_0 = (\alpha_1(0), \alpha_0(0), \phi(0), \omega(0), \hat{\theta}(0)) = (0.059 \text{ rad}, 0.059 \text{ rad}, 0.123 \text{ rad}, 0.062 \text{ rad/s}, 0.117 \text{ rad})$. It automatically finds that, for $T = 5.168$ s,

$$B(y_L, \delta(L)) \subseteq B(y_K, \delta(K)),$$

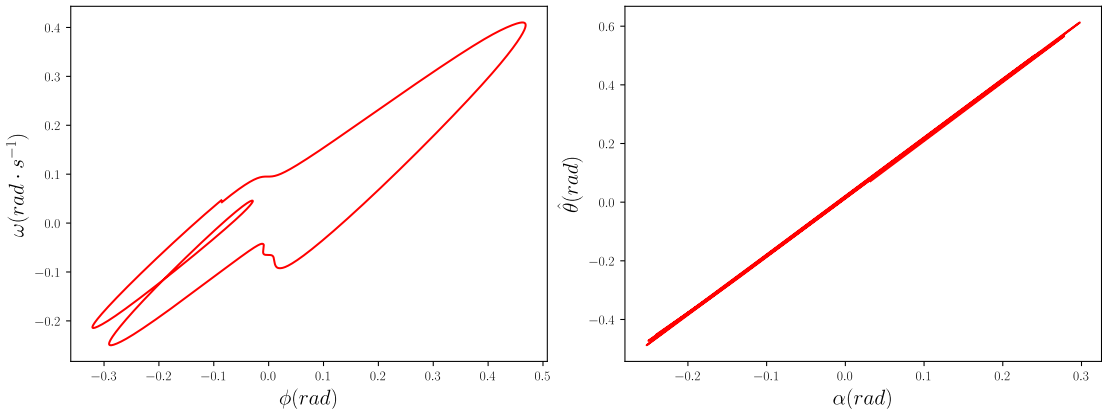

Figure 4: 2D projections of the limit cycle $\mathscr{C}$.

with $L = 10336$ and $K = 5168$. The associated limit cycle $\mathscr{C}$ and controlled invariant set $\mathscr{I}$ are depicted on Fig. 4 and Fig. 5 respectively, according to various 2D projections. In Fig. 5, the ball $B(y_K, \delta(K))$ is represented in orange, and the ball $B(y_L, \delta(L))$ in green (we see $B(y_L, \delta(L)) \subset B(y_K, \delta(K))$).

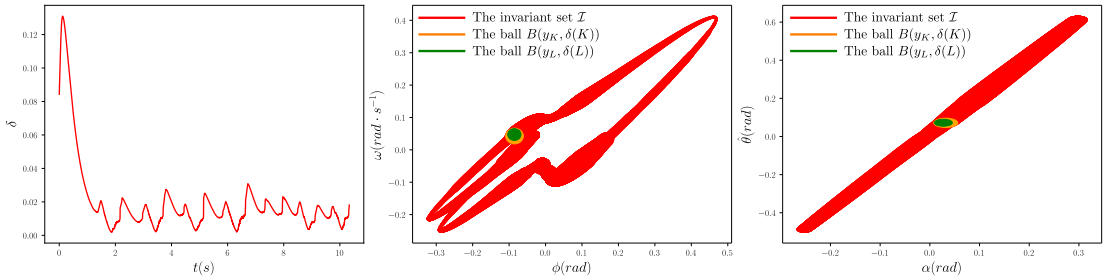

Figure 5: Evolution of the size $\delta(t)$ of the controlled invariant set $\mathscr{I}$ (top), followed by 2D projections of $\mathscr{I}$ for $\mathscr{W} = [\frac{-2\pi}{4000}, \frac{2\pi}{4000}]$.

4 Experimental results

4.1 Participants

One healthy right-handed adult took part in the experiments. A written consent was signed by the participant, and obtained as required by the Helsinki declaration [35]. The study was validated by a research ethics committee of Paris-Saclay (Université Paris-Saclay, 2021-303).

4.2 Kinematics

The kinematics of the human movement are measured by the opto-electronic motion capture device called "Qualysis". This system is composed of 10 cameras to capture the human movement at 179 Hz. There are 7 reflecting markers placed on the participant forearm, which allow the construction of plans based on the recommendations of *Ge Wu et al* [36]. The identification of the 7 markers is carried out using an AIM (Automatic Idenfication Markers) model on the Qualysis Track Manager software. In

order to make the participant do oscillatory movements, a sinusoidally moving target is projected on a screen in front of the subject.

4.3 Data acquisition

The code which controls the exoskeleton, also allows us to obtain its position as well as the parameters of Hopf oscillator. This allows to analyze the convergence of the oscillator. The data is first cleaned up, keeping only the part where the experiment starts.

4.4 Motor task

The participant is first placed in the robot at a distance from the targets corresponding to 2 times the size of his arm. The first three axis of the exoskeleton were mechanically blocked to avoid unwanted movement. Then a moving target is projected in a big screen in front of the participant. The target moves vertically with a varying sinusoidal trajectory. The participant is asked to follow the target by performing only the flexion/extension of the elbow. The pointing position is computed as the intersection between the line of the index and the plan of the screen, it is then projected in real time in the screen as a visual feedback for the participant. The subject starts with the forearm pointed at the fixed target in the middle (starting target) and then starts the experiment when the target starts to move as shown in Fig. 6.

The target follows the following sinusoidal trajectory :

$$\begin{aligned} x(t) &= A\sin(\omega t) \ , \\ A &= 0.3\ rad,\ \omega = 5\ \text{rad.s}^{-1} \ . \end{aligned} \tag{4}$$

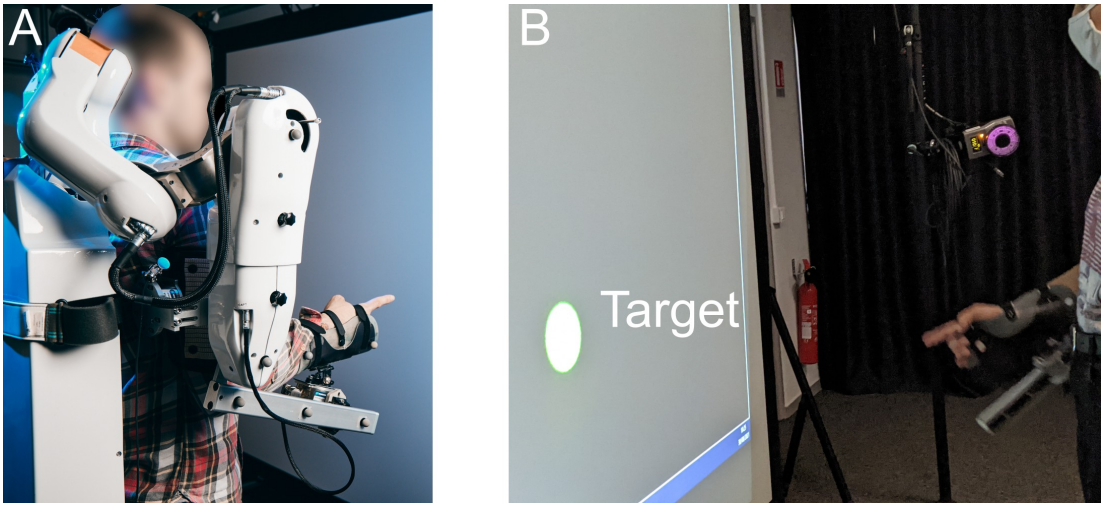

Figure 6: Description of the experimental setup. A: Markers on the forearms (human and exoskeleton). B: Target tracking example.

4.5 Experimental data

This section presents the behaviour of the set of states obtained in the experiment where we used the control scheme presented in Section 2.2. Fig. 7 represents the real position θ (also the oscillator input)

and the estimated position $\hat{\theta}$ computed by the oscillator. We can see that the estimation follows the desired position θ. We now compare the location of the experimental data with the invariant set $\mathscr{I}$

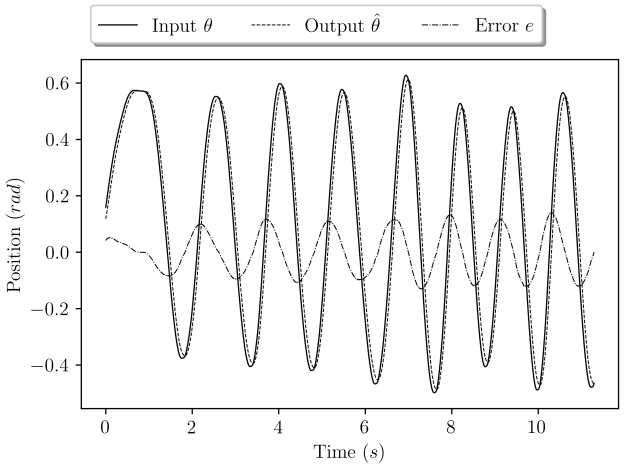

Figure 7: Evolution of the estimated position

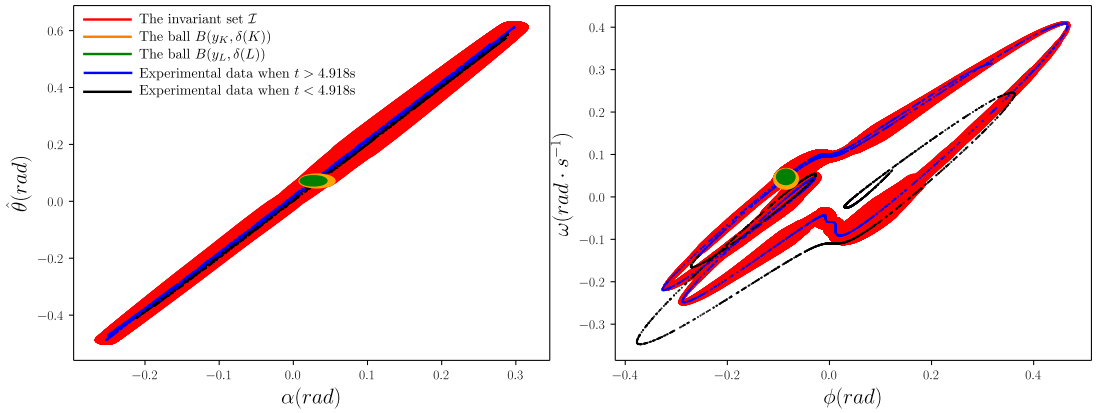

Figure 8: Evolution of the experimental data (black at $t < 4.918$ s then blue at $t \geq 4.918$ s) in the controlled invariant (red)

where $\mathscr{W} = [\frac{-2\pi}{4000}, \frac{2\pi}{4000}]$ constructed by reachability analysis in Section 3. Fig. 8 represents the set $\mathscr{I}$ together with 5000 points chosen randomly within the set of experimental data. At the beginning of the movement at $t < 4.918$ s, we see on Fig. 8 that the experimental points (black) are outside of the invariant set $\mathscr{I}$; then at $t \geq 4.918$ s the points (blue) are all located inside $\mathscr{I}$.

More precisely, there are in total 10336 experimental data points: 4918 points for $t < 4.918$ s and 5418 points for $t \geq 4.918$ s. All the 5418 points at $t \geq 4.918$ s are located inside the invariant set $\mathscr{I}$. For $t < 4.918$ s, the average of the distance between the experimental data and the limit cycle $\mathscr{C}$ is 0.0493 and the standard deviation 0.0255; for $t \geq 4.918$ s, the distance average is 0.0028 and the standard deviation 0.0023.

Fig. 9 shows the evolution of the distance between the experimental data and the limit cycle.

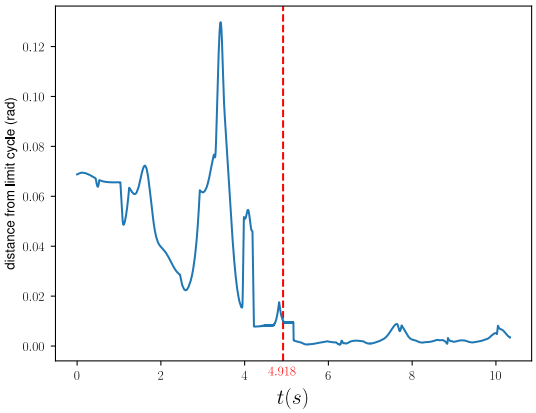

Figure 9: Evolution of the distance between the experimental data and the limit cycle.

As a conclusion, the experimental results allowed us to verify the efficiency of the Hopf oscillator on a complex robot such as ABLE.

5 Conclusion

We have described a methodology for

1. formally guaranteeing the convergence and robustness of the controlled system, at the model level, using a recent method of reachability analysis of periodic movements [18], and

2. verifying all these properties at the experimental level, via a protocol on human subjects.

In this pilot study we have verified that all the data of the experiments (after a possible transient phase) are located within the controlled invariant set $\mathscr{I}$ found, at the theoretical level, by reachability analysis (see Section 3). We are presently enriching the model by taking into account additional axes of movement, and considering more sophisticated adaptive oscillators than the Hopf oscillator. We think that the methodology presented here (relying on control with adaptive oscillators, and formal verification via reachability analysis) is still well-suited to the validation of such extensions.

References

[1] Arash Ajoudani, Andrea Maria Zanchettin, Serena Ivaldi, Alin Albu-Schäffer, Kazuhiro Kosuge, and Oussama Khatib. Progress and prospects of the human-robot collaboration. *Autonomous Robots*, pages 957–975, October 2018.

[2] Matthias Althoff, Goran Frehse, and Antoine Girard. Set Propagation Techniques for Reachability Analysis. *Annual Review of Control, Robotics, and Autonomous Systems* , 4(1), May 2021.

[3] Simon Bastide, Nicolas Vignais, Franck Geffard, and Bastien Berret. Interacting with a "transparent" upper-limb exoskeleton: a human motor control approach. *IEEE/RSJ International Conference on Intelligent Robots and Systems (IROS)*, pages 4661–4666, 2018.

[4] Franco Blanchini. Set invariance in control. *Automatica*, 35(11):1747–1767, 1999.

[5] Robert Bogue. Robotic exoskeletons: a review of recent progress. *Industrial Robot: An International Journal*, pages 5–10, January 2015.

[6] Michiel P. de Looze, Tim Bosch, Frank Krause, Konrad S. Stadler, and Leonard W. O'Sullivan. Exoskeletons for industrial application and their potential effects on physical work load. *Ergonomics*, 59(5):671–681, May 2016.

[7] Ryszard Dindorf and Piotr Wos. Using the bioelectric signals to control of wearable orthosis of the elbow joint with bi-muscular pneumatic servo-drive. 38(5):804–818, jul 2019.

[8] Laurent Fribourg. Euler's method applied to the control of switched systems. In *FORMATS*, volume 10419 of *LNCS*, pages 3–21. Springer, September 2017.

[9] Antonio Frisoli, Luigi Borelli, Alberto Montagner, Simone Marcheschi, Caterina Procopio, Fabio Salsedo, Massimo Bergamasco, Maria C. Carboncini, Martina Tolaini, and Bruno Rossi. Arm rehabilitation with a robotic exoskeleleton in Virtual Reality. In *IEEE 10th International Conference on Rehabilitation Robotics ICORR, 2007.*, pages 631–642, 2007.

[10] Antonio Frisoli, Caterina Procopio, Carmelo Chisari, Ilaria Creatini, Luca Bonfiglio, Massimo Bergamasco, Bruno Rossi, and Maria Chiara Carboncini. Positive effects of robotic exoskeleton training of upper limb reaching movements after stroke. *Journal of neuroengineering and rehabilitation*, 9(1):36, 2012.

[11] P. Garrec, J. P. Friconneau, Y. Méasson, and Y. Perrot. ABLE, an Innovative Transparent Exoskeleton for the Upper-Limb. *IEEE/RSJ International Conference on Intelligent Robots and Systems (IROS)*, pages 1483–1488, September 2008.

[12] Phillipe Garrec. Screw and Cable Acutators (SCS) and Their Applications to Force Feedback Teleoperation, Exoskeleton and Anthropomorphic Robotics. *Robotics 2010 Current and Future Challenges*, pages 167–191, 2010.

[13] R. A. R. C. Gopura, D. S. V. Bandara, Kazuo Kiguchi, and G. K. I. Mann. Developments in hardware systems of active upper-limb exoskeleton robots: A review. *Robotics and Autonomous Systems*, 75:203–220, jan 2016.

[14] Nathanael Jarrasse, Jamie Paik, Viviane Pasqui, and Guillaume Morel. How can human motion prediction increase transparency? *IEEE International Conference on Robotics and Automation*, pages 2134–2139, May 2008.

[15] Nathanaël Jarrasse and Guillaume Morel. Connecting a Human Limb to an Exoskeleton. *IEEE Transactions on Robotics*, 28(3):697–709, June 2012.

[16] Jawher Jerray. Orbitador: A tool to analyze the stability of periodical dynamical systems. In *ARCH*, 2021. To appear.

[17] Jawher Jerray and Laurent Fribourg. Determination of limit cycles using stroboscopic set-valued maps. In Raphaël M. Jungers, Necmiye Ozay, and Alessandro Abate, editors, *7th IFAC Conference on Analysis and Design of Hybrid Systems, ADHS 2021, Brussels, Belgium, July 7-9, 2021*, volume 54 of *IFAC-PapersOnLine*, pages 139–144. Elsevier, 2021.

[18] Jawher Jerray, Laurent Fribourg, and Étienne André. Robust optimal periodic control using guaranteed Euler's method. In *ACC*, pages 986–991. IEEE, 2021.

[19] Fabian Just, Özhan Özen, Stefano Tortora, Verena Klamroth-Marganska, Robert Riener, and Georg Rauter. Human arm weight compensation in rehabilitation robotics: efficacy of three distinct methods. *Journal of NeuroEngineering and Rehabilitation*, 17(1), feb 2020.

[20] Nili E. Krausz, Denys Lamotte, Iason Batzianoulis, Levi J. Hargrove, Silvestro Micera, and Aude Billard. Intent prediction based on biomechanical coordination of EMG and vision-filtered gaze for end-point control of an arm prosthesis. *IEEE Transactions on Neural Systems and Rehabilitation Engineering*, 28(6):1471–1480, jun 2020.

[21] Marie-Hélène Milot, Steven J Spencer, Vicky Chan, James P Allington, Julius Klein, Cathy Chou, James E Bobrow, Steven C Cramer, and David J Reinkensmeyer. A crossover pilot study evaluating the functional outcomes of two different types of robotic movement training in chronic stroke survivors using the arm exoskeleton BONES. *Journal of Neuroengineering and Rehabilitation*, 10(1):112, December 2013.

[22] Luke M Mooney, Elliott J Rouse, and Hugh M Herr. Autonomous exoskeleton reduces metabolic cost of human walking during load carriage. *Journal of NeuroEngineering and Rehabilitation*, 11(1):80, 2014.

[23] Jose L Pons. Rehabilitation exoskeletal robotics. *IEEE Engineering in Medicine and Biology Magazine*, 29(3):57–63, 2010.

[24] L. Righetti and Auke Jan Ijspeert. Programmable central pattern generators: an application to biped locomotion control. In *Proceedings of the 2006 IEEE International Conference on Robotics and Automation, ICRA*. IEEE, 2006.

[25] Ludovic Righetti, Jonas Buchli, and Auke Jan Ijspeert. Dynamic hebbian learning in adaptive frequency oscillators. *Physica D: Nonlinear Phenomena*, 216(2):269–281, apr 2006.

[26] Ludovic Righetti, Jonas Buchli, and Auke Jan Ijspeert. Adaptive frequency oscillators and applications. *The Open Cybernetics & Systemics Journal*, 3:64–69, oct 2009.

[27] Renaud Ronsse, Nicola Vitiello, Tommaso Lenzi, Jesse van den Kieboom, Maria Chiara Carrozza, and Auke Jan Ijspeert. Human–robot synchrony: flexible assistance using adaptive oscillators. *IEEE Transactions on Biomedical Engineering*, 58(4):1001–1012, apr 2011.

[28] André Schiele and Frans C. T. van der Helm. Influence of attachment pressure and kinematic configuration on pHRI with wearable robots. *Applied Bionics and Biomechanics*, 6(2):157–173, 2009.

[29] Nahema Sylla, Vincent Bonnet, Frédéric Colledani, and Philippe Fraisse. Ergonomic contribution of ABLE exoskeleton in automotive industry. *International Journal of Industrial Ergonomics*, 44(4):475–481, July 2014.

[30] Tatsuya Teramae, Tomoyuki Noda, and Jun Morimoto. EMG-based model predictive control for physical human–robot interaction: application for assist-as-needed control. *IEEE Robotics and Automation Letters*, 3(1):210–217, jan 2018.

[31] Benjamin Treussart, Franck Geffard, Nicolas Vignais, and Frederic Marin. Controlling an upper-limb exoskeleton by EMG signal while carrying unknown load. In *2020 IEEE International Conference on Robotics and Automation (ICRA)*, pages 9107–9113, may 2020.

[32] Dorian Verdel, Simon Bastide, Nicolas Vignais, Olivier Bruneau, and Bastien Berret. An identification-based method improving the transparency of a robotic upper limb exoskeleton. *Robotica*, 39(9):1711–1728, feb 2021.

[33] Ngoc Dung Vuong and Marcelo H. Ang Jr. Dynamic model identification for industrial robots. *Acta Polytechnica Hungarica*, 6(5):51–68, 2009.

[34] Wendong Wang, Lei Qin, Xiaoqing Yuan, Xing Ming, Tongsen Sun, and Yifan Liu. Bionic control of exoskeleton robot based on motion intention for rehabilitation training. *Advanced Robotics*, 33(12):590–601, June 2019. Publisher: Taylor & Francis _eprint: https://doi.org/10.1080/01691864.2019.1621774.

[35] World Medical Association. World Medical Association Declaration of Helsinki. Ethical principles for medical research involving human subjects. *Bulletin of the World Health Organization*, 79(4):373–374, 2001.

[36] Ge Wu, Frans C.T. van der Helm, H.E.J. (DirkJan) Veeger, Mohsen Makhsous, Peter Van Roy, Carolyn Anglin, Jochem Nagels, Andrew R. Karduna, Kevin McQuade, Xuguang Wang, Frederick W. Werner, and Bryan Buchholz. Isb recommendation on definitions of joint coordinate systems of various joints for the reporting of human joint motion—part ii: shoulder, elbow, wrist and hand. *Journal of Biomechanics*, 38(5):981–992, 2005.

[37] Yaguang Zhu, Yongsheng Wu, Qiong Liu, Tong Guo, Rui Qin, and Jizhuang Hui. A backward control based on σ-Hopf oscillator with decoupled parameters for smooth locomotion of bio-inspired legged robot. *Robotics and Autonomous Systems*, 106:165–178, August 2018.